Langmuir

Article

pubs.acs.org/Langmuir

Characterization of the Pore Structure of Three-Dimensionally Ordered Mesoporous Carbons Using High Resolution Gas Sorption

Katie A. Cychosz,[†] Xuefeng Guo,[‡,∥] Wei Fan,[‡,#] Richard Cimino,[§] Gennady Yu. Gor,[§,⊥] Michael Tsapatsis,[‡] Alexander V. Neimark,*[,§] and Matthias Thommes*[,†]

[†]Quantachrome Instruments, 1900 Corporate Drive, Boynton Beach, Florida 33426, United States

[‡]Department of Chemical Engineering and Materials Science, University of Minnesota, Minneapolis, Minnesota 55455, United States

[§]Chemical and Biochemical Engineering, Rutgers University, Piscataway, New Jersey 08854, United States

Supporting Information

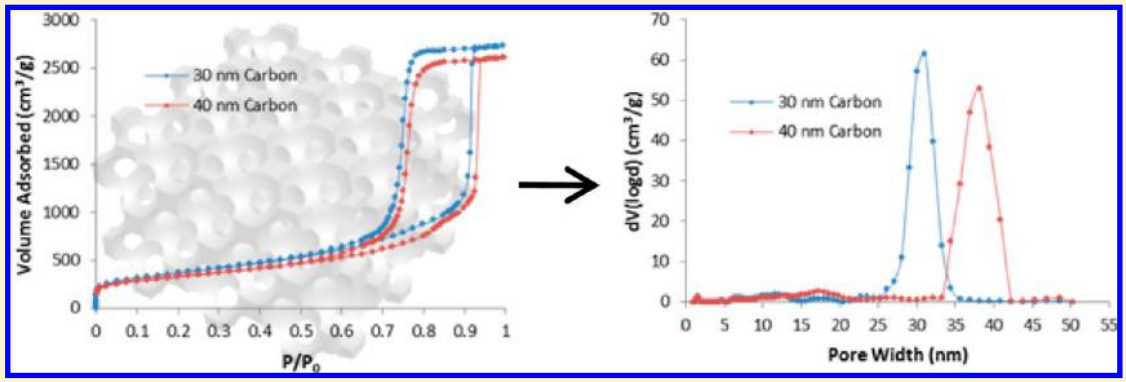

ABSTRACT: The use of colloidal crystals with various primary particle sizes as templates leads to the formation of three-dimensionally ordered mesoporous (3DOm) carbons containing spherical pores with tailorable pore size and extremely high pore volumes. We present a comprehensive structural characterization of these novel carbons by using nitrogen (77.4 K) and argon (87.3 K) adsorption coupled with the application of novel, dedicated quenched solid density functional theory (QSDFT) methods which assume correctly the underlying spherical pore geometry and also the underlying adsorption mechanism. The observed adsorption isotherms are of Type IV with Type H1-like hysteresis, despite the fact that pore blocking affects the position of the desorption branch. This follows also from detailed, advanced scanning hysteresis experiments which not only allow one to identify the underlying mechanisms of hysteresis, but also provide complementary information about the texture of these unique porous materials. This work addresses the problem of pore size analysis of novel, ordered porous carbons and highlights the importance of hysteresis scanning experiments for textural analysis of the pore network.

INTRODUCTION

Three-dimensionally ordered mesoporous (3DOm) carbons are obtained by templating colloidal crystals formed from lysine−silica nanoparticles. A schematic of the structure of a representative 3DOm carbon is shown in Figure 1 and the structure consists of spherically shaped pores connected by windows. Using colloidal crystals with various primary particle sizes (e.g., 10, 20, 30, 40 nm) allows one to accurately tailor the pore size of the 3DOm carbon.[1] Although precisely sized silica particles as small as 5 nm can be made, they have not yet been used for the fabrication of 3DOm carbon.[2] Templated 3DO-mesoporous or macroporous carbons are themselves used as a template for the confined synthesis of 3DOm-i (three-dimensionally ordered mesoporous-imprinted) zeolites,[3−5] nanostructured catalysts,[6,7] and other materials.[3,8] Pore sizes of previously synthesized 3DOm carbons were verified using techniques such as SEM and TEM. However, complete gas adsorption behavior including pore size/textural analysis of these 3DOm carbons is necessary in order to fully understand the properties and pore structure of these unique materials.

The development and availability of advanced theoretical approaches based on density functional theory (DFT) has led to major improvements in the characterization of porous materials.[9−15] Unlike classical methods based on the Kelvin equation, using DFT methods allows one to obtain an accurate pore size analysis over the complete pore size range using a single method. Nonlocal DFT (NLDFT) methods are now widely available for many adsorptive/adsorbent pairs and are featured in standards from the International Organization for Standardization (ISO) (ISO 15901-3). However, NLDFT methods do not take into account surface heterogeneity, which is typical for many porous materials. Most recently, quenched solid density functional theory (QSDFT), which

Received: June 11, 2012
Revised: July 18, 2012
Published: August 1, 2012

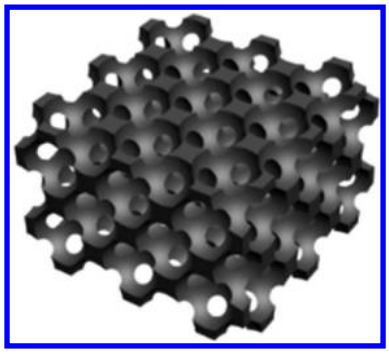

Figure 1. Representative three-dimensionally ordered mesoporous (3DOm) carbon structure.

does take into account the surface roughness of a material, has been developed and applied for pore structure characterization.[13,14] QSDFT was originally developed assuming slit-shaped pores which are typically found in activated microporous carbons. However, the emergence of novel materials with predesigned pore morphology (such as the 3DOm carbons) required the development of methods for carbons with cylindrical and spherical mesopore geometries. Recently, new QSDFT methods have been reported for the analysis of spherical mesopores, which are appropriate for characterization of various micro- and mesoporous carbons, including 3DOm carbons.[15]

In gas adsorption on mesoporous materials, the presence of hysteresis in the adsorption and desorption isotherms complicates the pore size analysis, but if interpreted correctly it can provide important information about the pore network. Identification of the underlying mechanism of hysteresis is sometimes quite difficult, and in such cases hysteresis scanning experiments[16−20] allow one to determine the mechanisms which are crucial to obtaining accurate characterization information. After the measurement of the initial adsorption/desorption curve, one measures in subsequent cycles the adsorption/desorption isotherm only in the relative pressure range where hysteresis occurs. For instance, after one has obtained the initial adsorption/desorption isotherm, one remeasures the adsorption branch only up to a relative pressure that is smaller than the saturation pressure. Consequently, only a portion of the pore system of the porous material has been filled with liquid before one starts with the desorption isotherm. This procedure is called *desorption scanning*. On the other hand, *adsorption scanning* is performed by increasing pressure from the desorption branch of the hysteresis loop. As a result, the shape of the scanning isotherms, as compared to the initial sorption isotherm, gives information about the specifics of adsorbate condensation and evaporation behaviors in the pores of the material (i.e., capillary evaporation vs pore blocking/percolation).

In this work, a systematic adsorption study has been performed including (i) high resolution nitrogen (77.4 K) and argon (87.3 K) sorption experiments over a wide range of relative pressures (P/P_0), that is, 10^{-7} to 1, (ii) accurate pore size analysis by applying QSDFT methods dedicated to nitrogen and argon adsorption in spherical carbon pores, and (iii) high resolution adsorption/desorption hysteresis scanning experiments on four representative 3DOm carbons templated

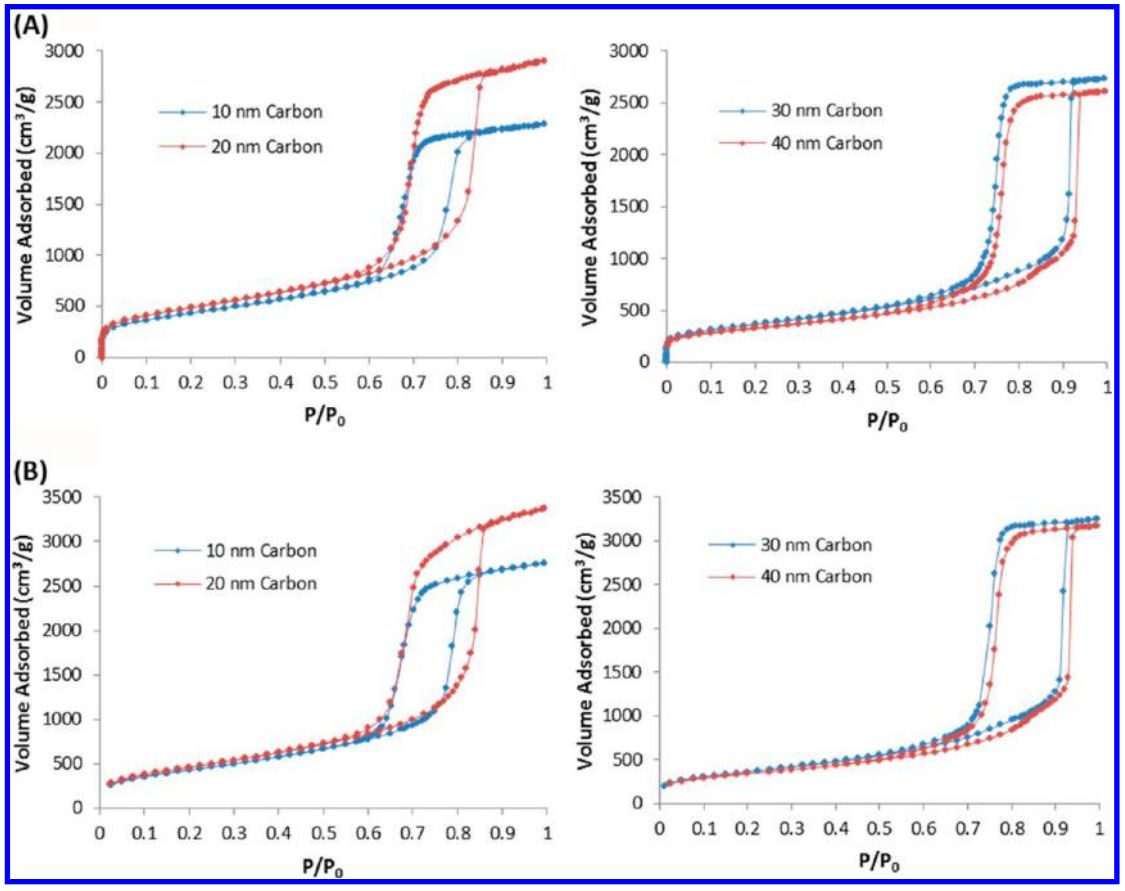

Figure 2. (A) Nitrogen (77.4 K) and (B) argon (87.3 K) adsorption isotherms.

dx.doi.org/10.1021/la302362h | *Langmuir* 2012, 28, 12647−12654

using 10, 20, 30, and 40 nm silica nanoparticles. These sized nanoparticles were chosen for convenience; however, intermediate sizes could be made as well.[21]

EXPERIMENTAL SECTION

Synthesis of Size-Tunable Lysine−Silica Nanoparticles and 3DOm Carbon. 3DOm carbons were prepared by the method reported by Yokoi and co-workers.[22] We further modified the method for making 3DOm carbons with larger cages.[1] Samples with various cage sizes were prepared by the replication of colloidal crystals composed of size tunable silica nanoparticles according to a previous report.[1] In detail, silica nanoparticle sols were synthesized by hydrolyzing tetraethyl orthosilicate (TEOS, 98%, Aldrich) in a lysine aqueous solution (Sigma-Aldrich) under continued magnetic stirring at 500 r.p.m for 48 h.[1,2,22] 10 and 20 nm silica nanoparticles were obtained at 60 and 90 °C, respectively, with a molar composition of 60 SiO_2/1.2 lysine/9500 water/240 ethanol. In order to make 30 and 40 nm silica nanoparticles, a seeded growth technique was employed in which the 20 nm particles were used as seeds. Subsequent repeated addition of TEOS, followed by growth at 90 °C for 24 h under vigorous stirring was carried out one time and three times to increase the particle size to 30 and 40 nm, respectively. The final molar compositions were 150 SiO_2/1.2 lysine/9500 water/600 ethanol for 30 nm and 490 SiO_2/1.2 lysine/9500 water/2940 ethanol for 40 nm. Colloidal crystal templates were formed by evaporation of the water from the lysine−silica nanoparticle sols in an oven at 70 °C for 24 h. Lysine was removed from the product by calcination at 550 °C for 12 h. Furfuryl alcohol (Aldrich) and oxalic acid (Aldrich) were used as carbon precursor and polymerization catalyst, respectively, for the synthesis of the 3DOm carbon. The replication was achieved by impregnating a solution containing furfuryl alcohol and oxalic acid with a molar ratio of 200/1 within the packed silica nanoparticles. The resulting product was heated to 90 °C for 1 day to allow the polymerization of furfuryl alcohol, then placed in flowing N_2, first at 200 °C for 3 h to cure the polymer and then heated at 900 °C for another 3 h to carbonize the polymer. The template silica nanoparticles were dissolved in 6 M KOH solution (Aldrich) at 180 °C for 3 days to yield the 3DOm carbon, which was then thoroughly washed with deionized water to near neutral pH.

SEM images were collected on a Hitachi S-900, equipped with a field-emission gun operated at 3.0 kV after the samples were coated by Pt.

Physical Adsorption Characterization. Adsorption experiments, including hysteresis scanning experiments, with nitrogen (77.4 K) and argon (87.3 K) were performed using a Quantachrome Autosorb iQ MP instrument. The 3DOm carbon samples were outgassed at 150 °C for 16 h under turbomolecular vacuum pumping prior to the gas adsorption measurements.

Characterization of the pore structure of these unique carbons was performed by applying novel QSDFT methods for nitrogen adsorption in spherical-pore carbons to the adsorption branch of the isotherms.[15] The QSDFT model developed and applied to these carbons is a hybrid model that assumes spherical pore geometry in the relative pressure range of hysteresis ($P/P_0 > 0.5$) and cylindrical pore geometry in the low pressure region ($P/P_0 < 0.5$). Furthermore, it takes correctly into account that pore condensation is delayed due to the existence of a metastable adsorption film and hindered nucleation of liquid bridges.

In addition, for comparison purposes, pore size distributions were also calculated from the adsorption branch of argon isotherms using a new QSDFT method developed for argon adsorption in spherical pore carbons, which is presented in this paper for the first time. More detailed information about this QSDFT method can be found in the Supporting Information.

RESULTS AND DISCUSSION

The measured nitrogen (77.4 K) and argon (87.3 K) high resolution adsorption/desorption isotherms for 3DOm carbons templated using 10, 20, 30, and 40 nm nanoparticles (hereafter referred to as the 10, 20, 30, or 40 nm carbon) (Figure 2) reveal interesting pore condensation and hysteresis behavior and are characterized by high surface areas and extremely large pore volumes. BET surface areas (calculated in the linear BET relative pressure range from 0.05 to 0.3) and pore volumes (calculated using the Gurvich rule at $P/P_0 = 0.95$) were determined from both the nitrogen and argon isotherms, and the data agree well (Table 1). In particular, the 20 nm carbon has a very large pore volume of 4.35 cm^3/g, indicating it may also be useful for storage applications where pore volume dictates ultimate storage capacity.

Table 1. BET Surface Areas and Pore Volumes for 3DOm Carbons

	S_{BET,N_2} (m^2/g)	$S_{BET,Ar}$ (m^2/g)	V_{pore,N_2} (cm^3/g)	$V_{pore,Ar}$ (cm^3/g)
10 nm carbon	1575	1591	3.54	3.49
20 nm carbon	1737	1757	4.35	4.35
30 nm carbon	1292	1318	4.20	4.15
40 nm carbon	1177	1221	4.01	4.00

The QSDFT results with regard to the pore size distribution and pore network morphology are in good agreement with the pore size expected due to the original nanoparticle template for each sample as shown in the representative SEM images (Figure 3). Figure 4 illustrates the pore size distributions obtained from the adsorption branches of the nitrogen and argon isotherms for the 3DOm carbons. Comparison of the nitrogen experimental isotherms with the theoretical QSDFT fitted isotherms plotted logarithmically indicates a good agreement between the model and the measured data (Figure S1). Cumulative pore volume plots have also been obtained from the QSDFT method for the nitrogen isotherms and are shown in Figure S2. Nitrogen pore volumes calculated from the QSDFT method are in good agreement with the pore volumes calculated using the Gurvich rule (shown in Table 1). Finally, we also observe agreement between the pore size distributions calculated from the nitrogen and argon isotherms using an appropriate QSDFT method for each adsorbate.

An important feature of these isotherms used for characterization of the 3DOm material is the hysteresis loop. According to IUPAC (1985),[23] the hysteresis loop correlates with the texture of the adsorbent, where Type H1 hysteresis is associated with a narrow distribution of cylindrical pores and Type H2 hysteresis is associated with more complex pore networks. As seen in Figure 2, the measured adsorption/desorption isotherms for the 3DOm carbons are Type IV isotherms with Type H1 hysteresis, which is typically observed for materials with cylindrical pores, although the main cavities of these carbons are known to be of spherical shape. Closer inspection of the isotherms reveals desorption behavior that is not typical of Type H1 hysteresis. In Figure 2, for both the nitrogen and argon isotherms, evaporation/desorption for the 10 and 20 nm carbons happens at the same relative pressure, indicating that the "windows" that are present in the porous carbon are the same size regardless of the size of the nanoparticle and the resulting cavity pore size and that the position of the desorption/evaporation branch does not reflect the equilibrium vapor−liquid phase transition which is typical for type H1 hysteresis.

Identification of the underlying mechanism of hysteresis is sometimes quite difficult, and in such cases hysteresis scanning

dx.doi.org/10.1021/la302362h | Langmuir 2012, 28, 12647−12654

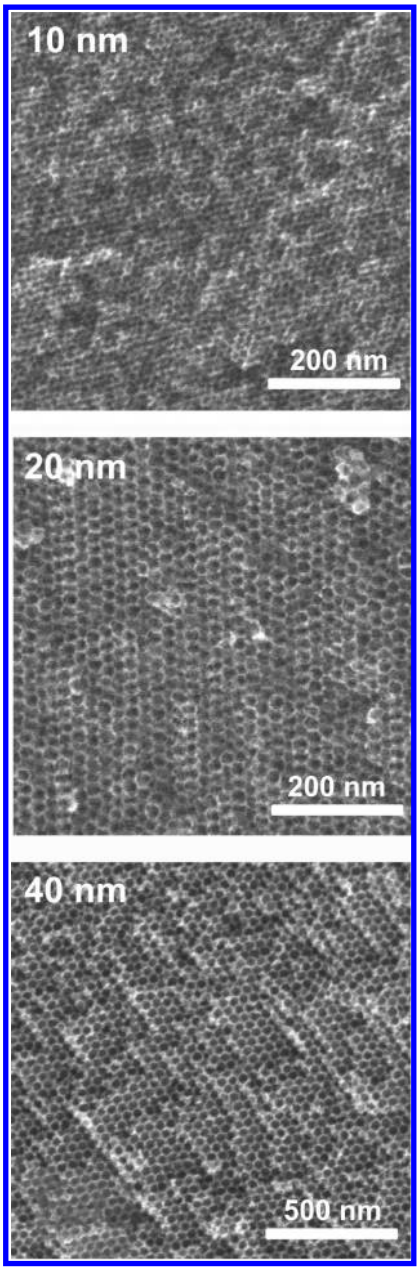

Figure 3. Representative SEM images of 10, 20, and 40 nm 3DOm carbons prepared by replication of colloidal crystals composed of lysine–silica nanoparticles.

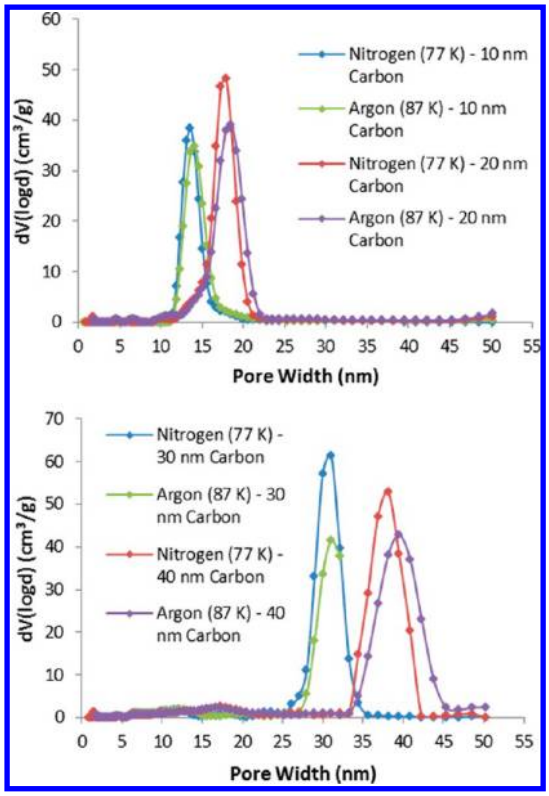

Figure 4. Pore size distributions calculated from the N_2 (77.4 K) and Ar (87.3 K) adsorption isotherms using QSDFT methods designed for carbons with spherical mesopores.

experiments, along with comparison of pore size distributions obtained using different adsorbates, allow one to distinguish the mechanisms, such as cavitation and pore blocking, which are crucial to obtaining accurate characterization information. A detailed analysis of the argon and nitrogen isotherms according to previously determined methods[12] reveals that cavitation does not contribute in an appreciable way to the observed hysteresis in the 3DOm carbons (Figure 5). It is known that cavitation induced evaporation occurs in ink-bottle type pores and is controlled by the state of the confined liquid and not by the width of the pore necks. As such, it is expected that if cavitation is present in the sample, the pore size distributions calculated using a proper method from the desorption branches of the nitrogen and argon isotherms should not agree at all; on the other hand, if pore blocking/percolation mechanisms are dominant, then the pore size distribution obtained from the desorption branches should agree because evaporation occurs at a relative pressure which is associated with the width of the pore neck.[12] Although the spherical pores in the 3DOm carbons are connected via windows rather than by necks, we assume here a desorption/evaporation mechanism characteristic of an ink-bottle geometry. As shown in Figure 5 for the 10 and 20 nm carbons, there is only a negligible difference between the nitrogen and argon pore size distributions, suggesting that cavitation cannot be the underlying evaporation mechanism. The controlling desorption mechanism depends on the pore sizes and, thus, is either equilibrium evaporation or pore blocking. This conclusion is confirmed also by the fact that the desorption for these carbons occurs at relative pressures ~0.6–0.7, which substantially exceed the values typically observed for cavitation (relative pressure of 0.45–0.5 for nitrogen).[12]

Further, the equilibrium desorption mechanism can also be excluded from consideration. Indeed, if the desorption branches would reflect an equilibrium liquid–vapor transition (which is typical for Type H1 hysteresis as mentioned before), the pore size distributions calculated from the adsorption branch (using a method that takes into account the delay in condensation) and the desorption branch (using an equilibrium method) should give identical pore size distributions. Because the 10 and 20 nm carbons have overlapping desorption branches, but nonoverlapping adsorption branches, the pore size distributions calculated from the adsorption and desorption branches do not overlap (see Figure 6 for examples of 10 and 40 nm carbon). This indicates that even though the isotherms look like Type H1 hysteresis, evaporation/desorption from the 3DOm carbon materials appears to occur via a pore blocking/percolation mechanism. In this case, the pore size distribution obtained

dx.doi.org/10.1021/la302362h | *Langmuir* 2012, 28, 12647–12654

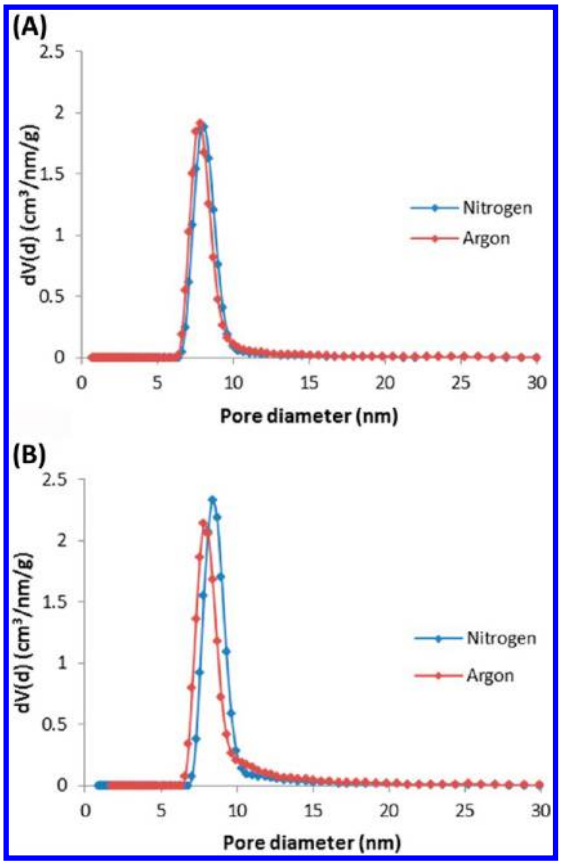

Figure 5. Nitrogen and argon QSDFT pore size distributions calculated from the desorption branch of the isotherms for (A) 10 nm 3DOm carbon and (B) 20 nm 3DOm carbon.

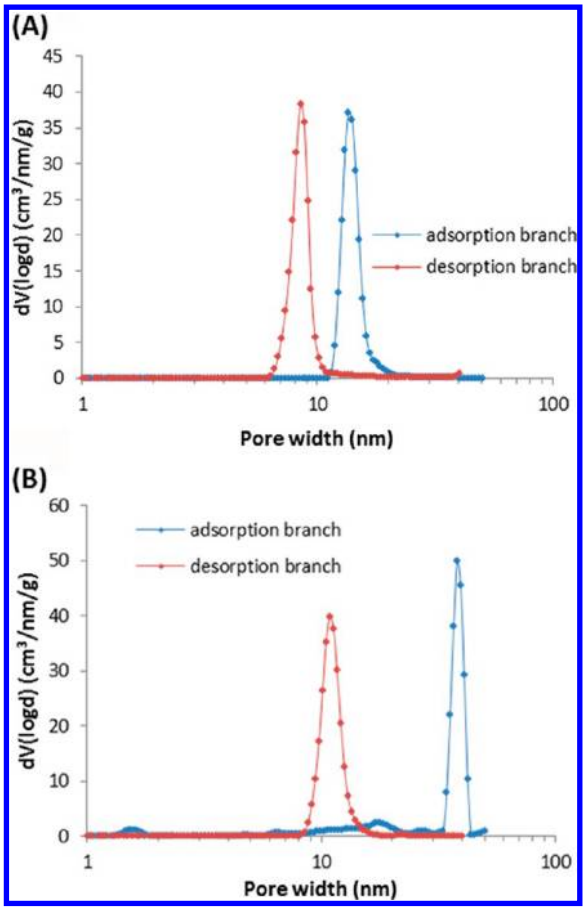

Figure 6. Pore size (cavity size) distributions calculated from the adsorption and window size from the desorption branches of the N_2 (77.4 K) isotherms for the (A) 10 nm 3DOm carbon and (B) 40 nm 3DOm carbon.

from the desorption branch is associated with the "window" sizes in the 3DOm carbon.

Why do we observe Type H1-like hysteresis although pore blocking/percolation effects are dominant here? The size distributions of pore cages and pore windows do not overlap and are both quite narrow (Figure 6). As such, these two distributions are likely weakly correlated. The assumption of the independent pore neck and pore body distributions was the foundation of the Everett theory of independent domains,[24] as well as site-bond percolation models,[16−18] which were used to explain the hysteresis and scanning isotherms in materials with Type H2 hysteresis. In so doing, the gradual adsorption branch of the Type H2 hysteresis loop was associated with a broad distribution of pore body sizes and the sharp adsorption branch with a cooperative percolation type desorption. In the case of the 3DOm carbons (templated with the regular assembly of monodisperse particles), the pore body size distribution is narrow, which brings about the Type H1 hysteresis loop with the adsorption branch as steep as the desorption branch. This conclusion is confirmed by analysis of hysteresis scanning isotherms presented below.

To further investigate the pore structure and origin of hysteresis, high resolution desorption scanning experiments[16−20,25−27] were performed for argon (87.3 K). The process of scanning desorption occurs when, during the course of an adsorption experiment, the relative pressure is changed from increasing to decreasing, in a manner similar to primary desorption. The shape and characteristics of the resulting scanning desorption isotherms can impart additional information about the system under consideration. In particular, desorption scanning isotherms provide a qualitative test of the importance of the effects of pore connectivity. In this respect, two extreme cases exist: the case of independent pores, in which the sorption behavior is determined by the pore width, and the disordered network case, in which percolation and pore blocking effects are dominant. The case of independent pores is frequently formulated in terms of deterministic models (DM). DM assumes that only the pore size determines the sorption properties of the system and it is thus a one parameter model. As such, there exists a one-to-one correspondence between adsorption and desorption pressures for a particular pore. Thus, for every partial pressure point $\chi_a = \chi_a(d_p)$, along the adsorption boundary curve there exists a companion point on the desorption boundary curve, $\chi_d = \chi_d(d_p)$. DM implies that adsorption and desorption scanning isotherms are reversible and cross the hysteresis loop between these points (Figure 7, left side), and as such, evaporation from a given pore does not depend on the state of neighboring pores. The correlation between these points is calculated from the condition of equality of the fractions of unfilled pores along the adsorption and desorption boundary curves. This behavior is expected for the samples exhibiting Type H1 hysteresis. It has also been shown that for samples where cavitation is the desorption mechanism, hysteresis scanning curves will also have the same shape, crossing the hysteresis loop, because desorption does not depend on the state of the neighboring pores.[28] In the other

dx.doi.org/10.1021/la302362h | *Langmuir* 2012, 28, 12647−12654

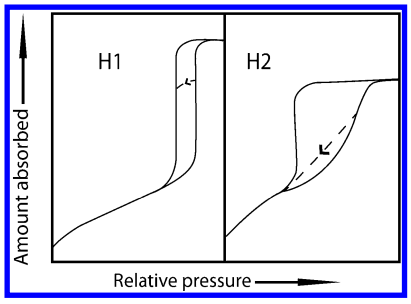

Figure 7. Examples of ideal desorption hysteresis scanning isotherms for Type H1 and Type H2 hysteresis. In Type H1 hysteresis, the scanning isotherm goes across the hysteresis loop. In Type H2 hysteresis, the scanning isotherm joins the desorption boundary isotherm at the lower closure point of hysteresis.

extreme case, that of a disordered network, quite different scanning behavior occurs. In disordered networks, there is a definite correlation between neighboring pores, with smaller pores effectively "blocking" the desorption of fluid from their larger neighbors which, without restriction, would have evaporated often at much higher partial pressures. During scanning desorption, the mesopores have access to the bulk vapor phase and can empty independently from each other due to the presence of initially unfilled neighboring pores. In this case, the desorption scanning curves will not cross the hysteresis loop, but instead will return to the boundary desorption curve at the lower closure point of hysteresis (Figure 7, right side). Hence, the scanning curves typically observed for Type H2 hysteresis do not follow the shape of the boundary desorption isotherm.

Argon desorption hysteresis scanning curves for the 10 and 40 nm 3DOm carbon are shown in Figure 8. The desorption scanning curves for the 10 nm sample clearly show behavior indicative of pore blocking effects; that is, the desorption scanning curves do not have the same shape or return immediately to the boundary desorption curve. The hysteresis scanning curves confirm that the emptying of pores in the 10 nm 3DOm carbon depends on the state of the neighboring pores. The desorption scanning curves for the 40 nm sample are in also in line with this explanation, but show a much more complex behavior.

To investigate the pore structure of these carbons even further, pore size distributions were calculated from each of the argon desorption scanning curves for the 10 and 40 nm carbons as shown in Figure 8. These pore size distributions reflect distributions of the maximum neck (connecting pore) size. For the 10 nm carbon, the window size distributions from the boundary curve and the desorption scanning curves all show a single, overlapping peak (Figure 8B) representative of the existence of a homogeneous pore system of "ink-bottle"-like pores which exhibit network effects on the desorption branch. The window size distributions from the desorption scanning curves of the 40 nm carbon (Figure 8D) show a more complicated pore structure comprised of two independent pore networks (labeled a and b in the figure). Because two peaks are

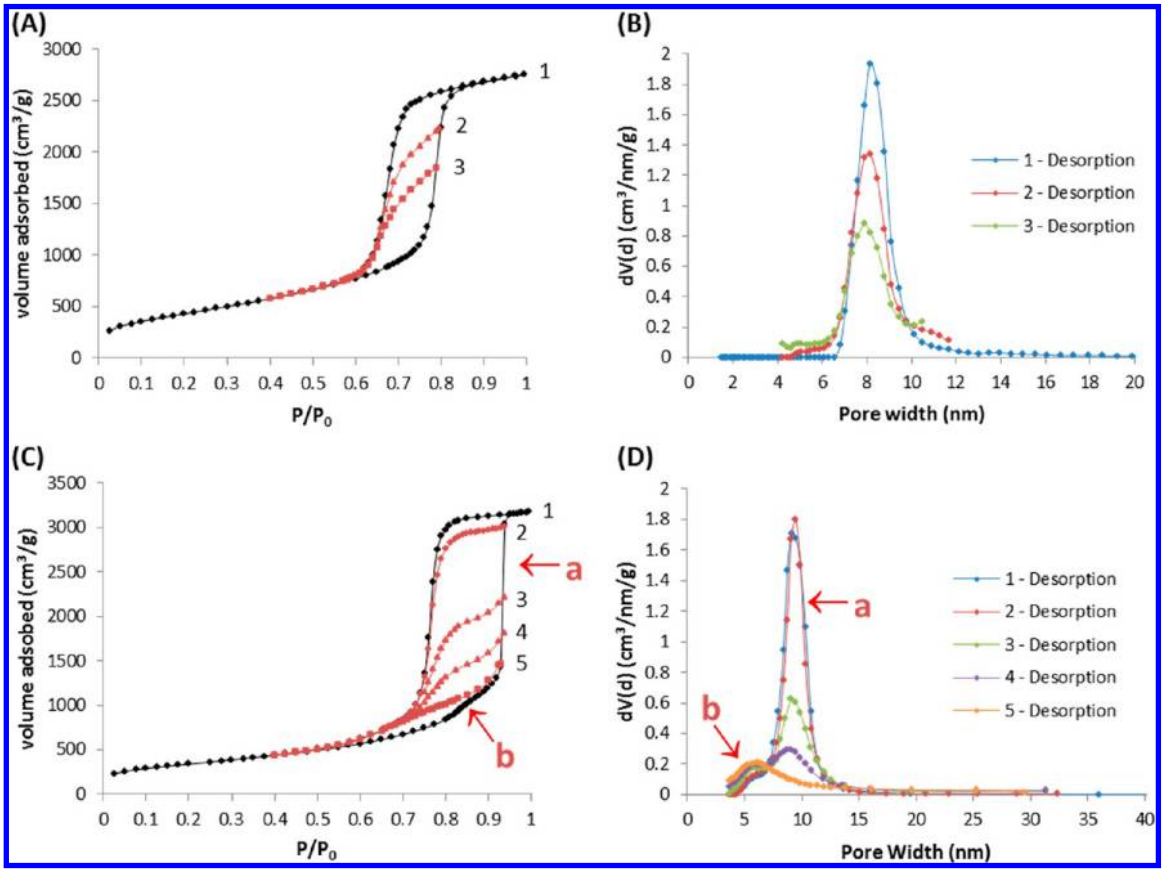

Figure 8. (A) Argon desorption scanning curves for the 10 nm 3DOm carbon, (B) distributions of the maximum neck size calculated form the desorption scanning curves for the 10 nm 3DOm carbon, (C) desorption scanning curves for the 40 nm 3DOm carbon, and (D) distributions of the maximum window size calculated from the desorption scanning curves for the 40 nm 3DOm carbon.

dx.doi.org/10.1021/la302362h | *Langmuir* 2012, 28, 12647−12654

observed, it can be concluded that these pore systems empty independently from one another and are, therefore, not interconnected. As mentioned above, the scan represented by "5" in Figure 8C is of completely different shape and behavior to the other hysteresis scans and, in this case, actually represents the boundary curve of the pore system b, because the pores of this pore system have been completely filled, but filling of pore system a has not yet begun. The formation of a secondary pore system can be explained by incomplete filling of the template with carbon precursor in the synthesis of the 3DOm carbon.

CONCLUSIONS

In summary, this work addresses the problem of the pore structure/size analysis of ordered carbons (3DOm carbons) consisting of spherical pores and highlights the importance of hysteresis scanning for textural analysis of the pore network. Well-defined, novel 3DOm carbons with spherical pores have been analyzed using nitrogen and argon adsorption, and structural information has been obtained through a QSDFT method that has been developed for carbons with spherical mesopores that takes correctly into account the delay in condensation. Combining nitrogen (77.4 K) and argon (87.3 K) adsorption with detailed hysteresis scanning experiments reveal that while adsorption does not depend on the state of neighboring pores, desorption is controlled by a classical pore blocking mechanism, despite the fact that Type H1 hysteresis is observed, which is usually associated with pore condensation/evaporation in cylindrical or slit-like pores. The observed Type H1 hysteresis can be associated with comparable width of the size distributions of cavities and windows. We performed comprehensive hysteresis scanning experiments which allow one to obtain detailed information about the pore network structure and its homogeneity which is inaccessible using other techniques, and reveals that in some of the 3DOm carbons there are two independent pore systems.

ASSOCIATED CONTENT

Supporting Information

Details of the QSDFT kernels, QSDFT fitted isotherms, and cumulative pore volume plots. This material is available free of charge via the Internet at http://pubs.acs.org.

AUTHOR INFORMATION

Corresponding Author

*E-mail: aneimark@rci.rutgers.edu (A.V.N.); matthias.thommes@quantachrome.com (M.T.).

Present Addresses

[‖]Lab of Mesoscopic Chemistry, School of Chemistry and Chemical Engineering, Nanjing University, Nanjing 210093, China.

[⊥]Department of Civil and Environmental Engineering, Princeton University, Princeton, NJ 08544.

[#]Department of Chemical Engineering, University of Massachusetts Amherst, Amherst, MA 01003.

Notes

The authors declare no competing financial interest.

ACKNOWLEDGMENTS

Materials synthesis for this work was supported as part of the Catalysis Center for Energy Innovation, an Energy Frontier Research Center funded by the U.S. Department of Energy, Office of Science, Office of Basic Energy Sciences under award number DE-SC0001004. A.V.N. acknowledges the ARO Grant W911NF-09-1-0242. A.V.N. acknowledges the ARO Grant 418 W911NF-09-1-0242 and support through the NSF ERC of Structured Organic Particulate Systems.

REFERENCES

(1) Fan, W.; Snyder, M. A.; Kumar, S.; Lee, P.-Y.; Yoo, W. C.; McCormick, A. V.; Penn, R. L.; Stein, A.; Tsapatsis, M. Hierarchical Nanofabrication of Microporous Crystals with Ordered Mesoporosity. *Nat. Mater.* **2008**, *7*, 984−991.

(2) Davis, T. M.; Snyder, M. A.; Krohn, J. E.; Tsapatsis, M. Nanoparticles in Lysine-Silica Sols. *Chem. Mater.* **2006**, *18*, 5814−5816.

(3) Yoo, W. C.; Kumar, S.; Penn, R. L.; Tsapatsis, M.; Stein, A. Growth Patterns and Shape Development of Zeolite Nanocrystals in Confined Syntheses. *J. Am. Chem. Soc.* **2009**, *131*, 12377−12383.

(4) Lee, P.-S.; Zhang, X.; Stoeger, J. A.; Malek, A.; Fan, W.; Kumar, S.; Yoo, W. C.; Al Hashimi, S.; Penn, R. L.; Stein, A.; Tsapatsis, M. Sub-40 nm Zeolite Suspensions via Disassembly of Three-Dimensionally Ordered Mesoporous-Imprinted Silicalite-1. *J. Am. Chem. Soc.* **2011**, *133*, 493−502.

(5) Chen, H.; Wydra, J.; Zhang, X.; Lee, P.-S.; Wang, Z.; Fan, W.; Tsapatsis, M. Hydrothermal Synthesis of Zeolites with Three-Dimensionally Ordered Mesoporous-Imprinted Structure. *J. Am. Chem. Soc.* **2011**, *133*, 12390−12393.

(6) Yokoi, T.; Sakuma, J.; Maeda, K.; Domen, K.; Tatsumi, T.; Kondo, J. N. Preparation of a Colloidal Array of $NaTaO_3$ Nanoparticles *via* a Confined Space Synthesis Route and Its Photocatalytic Application. *Phys. Chem. Chem. Phys.* **2011**, *13*, 2563−2570.

(7) Fukasawa, Y.; Takanabe, K.; Shimojima, A.; Antonietti, M.; Domen, K.; Okubo, T. Synthesis of Ordered Porous Graphitic-C3N4 and Regularly Arranged Ta3N5 Nanoparticles by Using Self-Assembled Silica Nanospheres as a Primary Template. *Chem.—Asian J.* **2011**, *6*, 103−109.

(8) Yoo, W. C.; Kumar, S.; Wang, Z.; Ergang, N. S.; Fan, W.; Karanikolos, G. N.; McCormick, A. V.; Penn, R. L.; Tsapatsis, M.; Stein, A. Nanoscale Reactor Engineering: Hydrothermal Synthesis of Uniform Zeolite Particles in Massively Parallel Reaction Chambers. *Angew. Chem., Int. Ed.* **2008**, *47*, 9096−9099.

(9) Lastoskie, C.; Gubbins, K. E.; Quirke, N. Pore Size Distribution Analysis of Microporous Carbons: A Density Functional Theory Approach. *J. Phys. Chem.* **1993**, *97*, 4786−4796.

(10) Neimark, A. V. The Method of Indeterminate Lagrange Multipliers in Nonlocal Density Functional Theory. *Langmuir* **1995**, *11*, 4183−4184.

(11) Ravikovitch, P. I.; Domhnaill, S. C. O.; Neimark, A. V.; Schueth, F.; Unger, K. K. Capillary Hysteresis in Nanopores: Theoretical and Experimental Studies of Nitrogen Adsorption on MCM-41. *Langmuir* **1995**, *11*, 4765−4772.

(12) Thommes, M.; Smarsly, B.; Groenewolt, M.; Ravikovitch, P. I.; Neimark, A. V. Adsorption Hysteresis of Nitrogen and Argon in Pore Networks and Characterization of Novel Micro- and Mesoporous Silicas. *Langmuir* **2006**, *22*, 756−764.

(13) Ravikovitch, P. I.; Neimark, A. V. Density Functional Theory Model of Adsorption on Amorphous and Microporous Silica Materials. *Langmuir* **2006**, *22*, 11171−11179.

(14) Neimark, A. V.; Lin, Y.; Ravikovitch, P. I.; Thommes, M. Quenched Solid Density Functional Theory and Pore Size Analysis of Micro-Mesoporous Carbons. *Carbon* **2009**, *47*, 1617−1628.

(15) Gor, G. Y.; Thommes, M.; Cychosz, K. A.; Neimark, A. V. Quenched Solid Density Functional Theory Method for Characterization of Mesoporous Carbons by Nitrogen Adsorption. *Carbon* **2012**, *50*, 1583−1590.

(16) Mason, G. The Effect of Pore Space Connectivity on the Hysteresis of Capillary Condensation in Adsorption-Desorption Isotherms. *J. Colloid Interface Sci.* **1982**, *88*, 36−46.

(17) Wall, G. C.; Brown, R. J. C. The Determination of Pore-Size Distributions from Sorption Isotherms and Mercury Penetration in Interconnected Pores: The Application of Percolation Theory. *J. Colloid Interface Sci.* **1981**, *82*, 141−149.
(18) Neimark, A. V. Percolation Theory of Capillary Hysteresis Phenomena and Its Application for Characterization of Porous Solids. *Stud. Surf. Sci. Catal.* **1991**, *62*, 67−74.
(19) Esparza, J. M.; Ojeda, M. L.; Campero, A.; Dominguez, A.; Kornhauser, I.; Rojas, F.; Vidales, A. M.; Lopez, R. H.; Zgrablich, G. N_2 Sorption Scanning Behavior of SBA-15 Porous Substrates. *Colloids Surf., A* **2004**, *241*, 35−45.
(20) Liu, H.; Zhang, L.; Seaton, N. Determination of the Connectivity of Porous Solids from Nitrogen Sorption Measurements − II. Generalisation. *Chem. Eng. Sci.* **1992**, *47*, 4393−4404.
(21) Snyder, M. A.; Lee, J. A.; Davis, T. M.; Scriven, L. E.; Taspatsis, M. Silica Nanoparticle Crystals and Ordered Coatings Using Lys-Sil and a Novel Coating Device. *Langmuir* **2007**, *23*, 9924−9928.
(22) Yokoi, T.; Sakamoto, Y.; Terasaki, O.; Kubota, Y.; Okubo, T.; Tatsumi, T. Periodic Arrangement of Silica Nanospheres Assisted by Amino Acids. *J. Am. Chem. Soc.* **2006**, *128*, 13664−13665.
(23) Sing, K. S. W.; Everett, D. H.; Haul, R. A. W.; Moscou, L.; Pierotti, R. A.; Rouquérol, J.; Siemieniewska, T. Reporting Physisorption Data for Gas/Solid Systems with Special Reference to the Determination of Surface Area and Porosity. *Pure Appl. Chem.* **1985**, *57*, 603−619.
(24) Everett, D. H. Adsorption Hysteresis. In *The Solid-Gas Interface*; Flood, E. A., Ed.; Marcel Dekker: New York, 1967; Vol. *2*, pp 1055−1113.
(25) Grossman, A.; Ortega, C. Capillary Condensation in Porous Materials. Hysteresis and Interaction Mechanism without Pore Blocking/Percolation Process. *Langmuir* **2008**, *24*, 3977−3986.
(26) Bruschi, L.; Fois, G.; Mistura, G.; Sklarek, K.; Hillebrand, R.; Steinhard, M.; Gösele, U. Adsorption Hysteresis in Self-Ordered Nanoporous Alumina. *Langmuir* **2008**, *24*, 10936−10941.
(27) Tompsett, G. A.; Krogh, L.; Griffin, D. W.; Conner, W. C. Hysteresis and Scanning Behavior of Mesoporous Molecular Sieves. *Langmuir* **2005**, *21*, 8214−8225.
(28) Rasmussen, C. J.; Vishnyakov, A.; Thommes, M.; Smarsly, B. M.; Kleitz, F.; Neimark, A. V. Cavitation in Metastable Liquid Nitrogen Confined to Nanoscale Pores. *Langmuir* **2010**, *26*, 10147−10157.